Battlefield Weapons Systems
& Technology, Volume X

MILITARY BALLISTICS

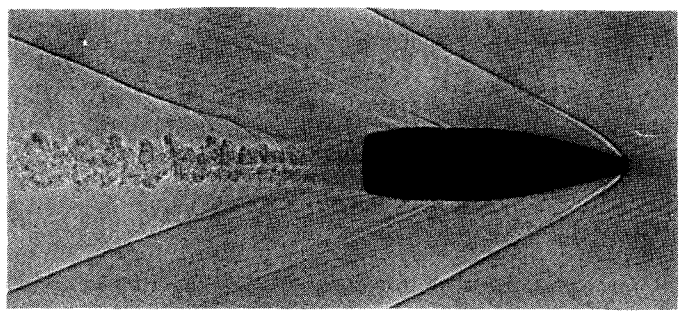

A Basic Manual

Contents

List of Illustrations		ix
Chapter 1	History of Ballistics	1
Chapter 2	Internal Ballistics - Part I	9
	Internal Ballistics - Part II	39
Chapter 3	Intermediate Ballistics	53
Chapter 4	External Ballistics - Part I	71
	External Ballistics - Part II	103
Chapter 5	Terminal Ballistics - Part I	137
	Terminal Ballistics - Part II	153
Chapter 6	Wound Ballistics	161
Chapter 7	Ballistics Instrumentation	173
Answers to Self Test Questions		201
Bibliography		207
Index		209

List of Illustrations

Chapter 1

FIG 1.1 Ballista 2

Chapter 2 - Part I

FIG 2.1 The main ballistic components of the loaded gun 10

FIG 2.2 105 mm shell featuring a single driving band 11

FIG 2.3 7.62 x 51 mm cartridge together with a fired boattailed bullet and an unfired flat-based bullet 12

FIG 2.4 105 mm calibre APFSDS (Armour Piercing Fin-Stabilised Discarding Sabot) with sabot attached 12

FIG 2.5 Cross-section of a shotgun cartridge 13

FIG 2.6 Common shapes of propellant granules 14

FIG 2.7 Preparation of smokeless propellants 14

FIG 2.8 Three stages in the burning of a cylindrical propellant granule 15

FIG 2.9 Ignition temperature of smokeless propellants 15

FIG 2.10 Typical burning rate constants 16

FIG 2.11 Burning rate against pressure for a typical propellant 16

FIG 2.12 Pressure within a closed-vessel plotted against time 17

FIG 2.13 Typical adiabatic (closed-vessel) flame temperatures 18

FIG 2.14 Examples of ballistic size 18

FIG 2.15 Types of progressive granules 19

FIG 2.16 Cross-sections of 7 hole multi-tube granule 20

FIG 2.17 Examples of granule shapes and their form function coefficients 20

FIG 2.18 Configuration of igniter and propellant charge in typical ammunition 21

FIG 2.19 Typical pressure/time, velocity/time and travel/time curves 23

FIG 2.20 Typical pressure/space and velocity/space curves 23

FIG 2.21 The four factors which determine projectile acceleration 24

FIG 2.22 Typical frictional force during firing 24

FIG 2.23 The approximate distribution of liberated energy 25

FIG 2.24 Approximate recoil energies relative to total available energy 25

FIG 2.25 Examples of peak pressure 26

FIG 2.26 Pressure/space curves for three full charges of propellant 28

FIG 2.27 Erosion of the gun 29

FIG 2.28 An eroded gun sectioned to show enlargement of the bore and worn rifling 30

FIG 2.29 Cross-section of the bore and relative rates of erosion 31

FIG 2.30 Rifling depth in a Probertised barrel 32

FIG 2.31 Examples of practical barrel life 32

FIG 2.32 Chieftain tank fitted with 120 mm lagged gun 33

FIG 2.33 The principle of the recoilless jet reaction gun 34

FIG 2.34 LAW 80 (early model) anti-tank recoilless rocket launcher (Photo by courtesy of Hunting Engineering Ltd) 34

FIG 2.35 120 mm Conbat recoilless jet reaction gun 34

Chapter 2 - Part II

FIG 2.36 Flow diagram for a lumped parameter computer model of internal ballistics, with description given on left hand side 50

Chapter 3

FIG 3.1	Shock waves formed by the release of high pressure gas from a muzzle	55
FIG 3.2	Shock wave formation before projectile exit	56
FIG 3.3	The precursor blast field of a 5.56 mm calibre rifle	56
FIG 3.4	The initial formation of shock waves shortly after projectile exit	57
FIG 3.5	Expansion of the blast field	58
FIG 3.6	Final phase of the blast field before contraction of the bottle shock and Mach disc	58
FIG 3.7	Preflash	59
FIG 3.8	Flash	60
FIG 3.9	The intense secondary flash of a 120 mm calibre Chieftain tank gun (Photo by courtesy of T. D. and P. W. Royal Armoured Corps, Bovington Camp)	60
FIG 3.10	The intense secondary flash from the breech nozzle of a 120 mm calibre Wombat recoilless gun	61
FIG 3.11	The primary and intermediate flash of a 7.62 mm calibre rifle showing the total absence of secondary flash	61
FIG 3.12	Conical, slotted tube and bar type flash suppressors on 5.56 mm calibre rifles	62
FIG 3.13	Cross-section of an idealised shock wave	63
FIG 3.14	Table of overpressures in atmospheres against intensity of sound in decibels (reference pressure 2×10^{-5} Pascals)	64
FIG 3.15	Methods of blast suppression	65
FIG 3.16	9 mm calibre sten sub machine gun fitted with silencer	65
FIG 3.17	The principle of the muzzle brake	67
FIG 3.18	Muzzle brake fitted to British 105 mm calibre light gun	68

Chapter 4 - Part I

FIG 4.1	Motion of a projectile under no external influences	72
FIG 4.2	Motion of a projectile under the action of gravity	72
FIG 4.3	Compression waves at subsonic speed	73
FIG 4.4	Shock wave at supersonic speed	74
FIG 4.5	Shadowgraph of 7.62 mm bullet (Photo by courtesy of RMCS Shrivenham)	75
FIG 4.6	Shadowgraph of high drag training round (Photo by courtesy of RMCS Shrivenham)	75
FIG 4.7	Shadowgraph of space re-entry model showing detached shock wave	76
FIG 4.8	Base drag	77
FIG 4.9	Air resistance	78
FIG 4.10	Real and in-vacuo trajectories	79
FIG 4.11	The effect of air resistance on certain projectiles	80
FIG 4.12	Calibre radius head	81
FIG 4.13	Fractional calibre radius head	81
FIG 4.14	Boattail design	82
FIG 4.15	The variation of C_D with speed in the subsonic region for different nose shape projectiles	83
FIG 4.16	The variation of C_D with speed for two differently shaped projectiles	84
FIG 4.17	The variation of C_D with speed for a typical shell	84
FIG 4.18	The effect of base bleed on range	85
FIG 4.19	Angle of yaw	86
FIG 4.20	Over-turning moment	86
FIG 4.21	Stability of an arrow	87
FIG 4.22	British 81 mm mortar bomb (Photo by courtesy of RMCS Shrivenham)	88

FIG 4.23 Gyroscopic motion 89

FIG 4.24 Precession and nutation for a spinning projectile 89

FIG 4.25 Over-stabilised shell 90

FIG 4.26 Gyroscopic forces acting on a spinning top 91

FIG 4.27 Rear view of spinning projectile : nose movement to the right 91

FIG 4.28 Rear view of spinning projectile : nose movement downwards 92

FIG 4.29 Rear view of spinning projectile : nose movement to the left 92

FIG 4.30 Equilibrium yaw 93

FIG 4.31 Magnus effect 93

FIG 4.32 Variation of P, ρ, T and ν with altitude 96

FIG 4.33 Extension of range when firing eastward at low elevation 98

Chapter 4 - Part II

FIG 4.34 Parabolic motion in vacuo 104

FIG 4.35 The effect of gravity and drag acting on a projectile 105

FIG 4.36 Conservation of linear momentum 106

FIG 4.37 Some exhaust velocities and specific impulses for various types of propellant 108

FIG 4.38 Rocket trajectories 109

FIG 4.39 Dynamic similarity 112

FIG 4.40 The relationship between C_D and Re 113

FIG 4.41 Viscous boundary layer 114

FIG 4.42 Boundary layer separation 116

FIG 4.43 Wind-axes 117

FIG 4.44 Body-axes 118

FIG 4.45 Variation of C_D with angle of yaw 119

FIG 4.46 Variation of C_L with angle of yaw 119

FIG 4.47 Variation of C_M with angle of yaw 120

FIG 4.48 Spinning top 121

FIG 4.49 Angular velocities of spinning top 122

FIG 4.50 Resolved components of angular velocities 123

FIG 4.51 Two arm model applied to spinning top 126

FIG 4.52 Forces acting on a spinning shell 127

FIG 4.53 Variation of C_{M_α} with M 128

FIG 4.54 Two arm model applied to spinning projectile 129

FIG 4.55 Typical patterns for aerodynamically stable projectiles 130

FIG 4.56 Typical patterns for aerodynamically unstable projectiles 130

FIG 4.57 Rosette motion 131

FIG 4.58 Equilibrium yaw motion 131

FIG 4.59 Increments of angular momentum 132

FIG 4.60 Equilibrium yaw angle 133

Chapter 5

FIG 5.1 Angle of attack 138

FIG 5.2 Impact of a long rod penetrator 141

FIG 5.3 Perforation mechanisms 142

FIG 5.4 Basic components of an APDS projectile 144

FIG 5.5 Basic components of an APFSDS projectile 145

FIG 5.6 Basic components of a HE fragmentation shell 145

FIG 5.7 The shaped charge principle 147

FIG 5.8 Penetrative performance of a conical liner 147

FIG 5.9 Basic components of a HEAT projectile 148

FIG 5.10 HEAT effect 149

FIG 5.11 Basic components for a HESH projectile 150

FIG 5.12 HESH effect 150

Chapter 6

FIG 6.1 Wound track of subsonic projectile 162

FIG 6.2 Stress wave formed by high velocity projectile 162

FIG 6.3 Temporary cavity formed by high velocity projectile 163

FIG 6.4 Selected stills from a high speed cine film showing the temporary cavitation (Photo by courtesy of CDE, Porton Down) 164

FIG 6.5 The respective wounding effects of a soft bullet, unstable jacketed bullet and stable jacketed bullet 165

FIG 6.6 The permanent record of cavitation effects as shown in standard soap blocks (Photo by courtesy of CDE, Porton Down) 165

FIG 6.7 Possible cavitation effects with metallic armour 167

FIG 6.8 The non-penetrating impact of a 9 mm bullet travelling at 330 m/s against 16 plys of Kevlar body armour (Photo by courtesy of CDE, Porton Down) 168

Chapter 7

FIG 7.1 Time scale for various illuminating sources 174

FIG 7.2 A microflash photograph of a 105 mm shell in flight (Photo by courtesy of RMCS Shrivenham) 174

FIG 7.3 A microflash photograph of 120 mm APDS in flight (Photo by courtesy of P. Fuller, RARDE) 175

FIG 7.4 Experimental arrangement for spark photography 176

FIG 7.5 Diagrammatic representation of the shadowgraph 176

FIG 7.6 Multiple spark photograph (Photo by courtesy of P. Fuller, RARDE) 177

FIG 7.7 Schlieren photograph of sphere (Photo by courtesy of P. Fuller, RARDE) 177

FIG 7.8	The Schlieren system	178
FIG 7.9	Rocket launching (Photo by courtesy of P. Fuller, RARDE)	179
FIG 7.10	Compensation for film movement by rotating glass block	180
FIG 7.11	Ballistic synchro technique (Diagram by courtesy of P. Fuller, RARDE)	181
FIG 7.12	A ballistic synchro record of 120 mm APDS (Photo by courtesy of P. Fuller, RARDE)	181
FIG 7.13	The rotating mirror streak camera (Diagram by courtesy of P. Fuller, RARDE)	182
FIG 7.14	The rotating mirror framing camera (Diagram by courtesy of P. Fuller, RARDE)	182
FIG 7.15	Image converter camera schematic	183
FIG 7.16	Lead pellet impacting on hard target (Photo by courtesy of John Hadland Photographic Instrumentation Ltd., Herts, UK)	183
FIG 7.17	Streak photograph of 7.62 mm bullet travelling at approximately 840 m/s (Photo by courtesy of RMCS Shrivenham)	184
FIG 7.18	X-ray shadowgraph of 0.45 automatic during firing (Photo by courtesy of Hewlett Packard Ltd., Berks, UK)	184
FIG 7.19	PCC equipment	186
FIG 7.20	Principle of radio-doppler	187
FIG 7.21	Principle of yaw sonde	188
FIG 7.22	Principle of the 'V' cell	189
FIG 7.23	Interpretation of pulse record	189
FIG 7.24	Results from yaw sonde	190
FIG 7.25	Shot position indicator (Photo by courtesy of M.S. Instruments Ltd., Kent, UK)	191
FIG 7.26	Position of shock wave front	191
FIG 7.27	Cartesian co-ordinate system	192

FIG 7.28 Crusher gauge 193

FIG 7.29 Basic interferometer system 195

FIG 7.30 Direct optical method 196

FIG 7.31 Bore-wire resistance method 196

FIG 7.32 Linear displacement transducers 197